Time Series approach to map areas of Agricultural Plastic Waste generation

Marlon F. de Souza [1], Rubens A.C. Lamparelli [1], João P.S. Werner [2], Murilo H.S. de Oliveira [1], Telma T. Franco [1,3]

[1] Universidade Estadual de Campinas (Unicamp), Center for Energy Planning (NIPE), Campinas, Brazil – marlonf@unicamp.br; lamparel@unicamp.br; m185795@dac.unicamp.br
[2] Unicamp, School of Agricultural Engineering, Campinas, Brazil – j164880@dac.unicamp.br
[3] Unicamp, Chemical Engineering, Campinas, Brazil – tfranco@unicamp.br

Keywords: Remote Sensing, plastic mulching, sits, Sentinel-2, Plastic-Mulched Farmland (PMF), deep learning.

Abstract

The escalating presence of plastics in agriculture has raised concerns regarding Agricultural Plastic Waste (APW). Hitherto, a lack of comprehensive plasticulture data impedes effective waste management strategies, potentially resulting in plastic pollution and contributing to microplastic formation. APW locations and quantities are pivotal for territorial planning and the formulation of public policies on waste management and land use. Remote detection of agri-plastics has garnered increased consideration, particularly in mapping plastic-mulched farmlands (PMFs) dispersed in extensive regions. This study investigates whether the use of satellite image time series can map PMFs accurately. We assessed pixel-based classification using a 16-day composite time series of Sentinel-2 imagery (S2-16D) obtained from the Brazil Data Cube project. The Plastic-Mulched Landcover Index (PMLI) was joined into S2-16D bands because it is an index focused on PMF detection. Four classifiers (RF, MLP, L-TAE, and TCNN) were compared through agreed classification metrics. The most promising outcome showed an overall accuracy of 100% employing L-TAE but with visible noise in the map. The time series enhanced accuracy while minimizing background confusion, offering a viable solution for PMF detection. The PMF map presented herein represents an initial stride toward fostering circularity in plasticulture throughout South America.

1. Introduction

Plastic pollution and climate change are two global sustainability challenges rooted in the exploitation of fossil carbon (Ni et al., 2021). The plastic-covered agriculture, known as plasticulture, is part of the transformation of agriculture into something more industrial and high-tech, changing the appearance of agricultural landscapes (Levin et al., 2007). Mapping agri-plastic and monitoring post-use fate are substantial challenges, mostly when plastic is dispersed in extensive regions or the use is very intensive (Perilla & Mas, 2019).

The utilization of plasticulture has expanded significantly because of the continued demand for food production globally (United Nations, 2021). Given the ongoing growth in world population and anticipated climate changes, this trend may continue. Plastic is key in many agricultural applications, contributing significantly to yield improvements (Gao et al., 2022). However, the increasing ubiquity of plastic in the agricultural production chain has resulted in increased environmental leakage (Food and Agriculture Organization, 2021; Ghaffar et al., 2022). Plastic is remarkably versatile despite being predominantly single-use. Plastic debris can pose potential hazards to biotic systems (Huo et al., 2022), rendering agricultural plastic waste (APW) a pressing global concern (Ghaffar et al., 2022).

Classifying Earth Observation (EO) imagery for mapping plastic greenhouses (PGHs) plastic-mulched farmlands (PMFs) presents challenges due to spatial resolution limitations, variations in pigment and spectral properties, and false detection issues close to urban areas (P. Zhang et al., 2022; D. Chen et al., 2023; de Souza et al., 2024).

As chronological sequence may be appropriate to reduce PMF misclassification, this article aims to test whether the use of satellite image time series can accurately map PMF. We compared four classification algorithms using the Sentinel-2-16D data cube (Simoes et al., 2021) with the incorporation of one plastic index. Lastly, we cared about model scalability to enable the production of additional plasticulture maps for Brazil.

Detecting tomato PMF is a difficult task in remote sensing (RS) due to the dynamic nature of agricultural practices, which results in considerable spatial mobility (de Souza et al., 2024). Farmers rotate their tomato crop site every season to prevent pest infestations and disease, alternating with annual crops or grazing fields. This rotation, while beneficial for crop health, intensifies the production of APW. Nevertheless, it is necessary to curb plastic pollution from agriculture (Hofmann et al., 2023). Our focus addresses the critical issue of PMF mapping. We expect that this paper can contribute to further comprehension of characteristics and essential attributes in plastic classification, technically evolving this RS field. The time-series approach is a good proposal for reducing erroneous classification and improving accuracy, as recently presented by de Souza et al. (2024).

1.1 Sustainability and plastic residue concerns in Brazil

There is a significant gap in information on Brazilian plasticulture, especially regarding post-use. Even though concerns about the post-use of APW and the recent rise of agricultural plastic remote mapping worldwide (Veettil et al., 2023). The Campo Limpo initiative stands as a good model of reverse logistics excellence for the disposal of pesticide containers (Institute for Processing Empty Packages - inpEV, 2023). However, a comparable scheme for retrieving plastic films remains absent. Moreover, the scarcity of comprehensive information about the plasticulture chain hinders the development of effective circular economy strategies.

1.2 New technologies to map plastic in agriculture

The machine learning (ML) advance has pivoted to a new era of image big data analytics. Deep learning (DL) approaches have been at the forefront of these efforts (Dimitrovski et al., 2023). Performance on many EO tasks has improved significantly (Veettil et al., 2023). As plastic becomes increasingly important

This contribution has been peer-reviewed. The double-blind peer-review was conducted on the basis of the full paper.
https://doi.org/10.5194/isprs-annals-X-3-2024-101-2024 | © Author(s) 2024. CC BY 4.0 License.

in agriculture, RS imagery has emerged as a key asset for quantifying agricultural plastic (Hasituya et al., 2017; Liu & Xin, 2023; Veettil et al., 2023).

1.3 Related Work

The first works related to the remote detection of agri-plastics emerged in the 2000s. Zhao et al. (2004), Levin et al. (2007), and Agüera et al. (2008) presented good approaches for agri-plastic mapping using satellite images. However, over the last few years, the focus changed to the recent use of computer vision techniques and DL models.

Our literature review showed that many recent methods have been developed to efficiently and accurately map various types of plastic waste, including potential generation sources in urban and rural areas. For example, Blanco et al. (2018) presented a GIS-based method to map APW. Afxentiou et al. (2021) published a PGH APW mapping database. Hong et al. (2023) proposed a method for simultaneously extracting the number and area of PGH. Kruse et al. (2023) used neural networks in Sentinel-2 data to identify terrestrial aggregations of plastic waste. Lin et al. (2023) proposed an adapted version of YOLOv5 to detect film debris in agricultural fields by using attention and replacing spatial pyramid pooling (SPPF) with an adaptive multi-scale fusion module. However, some gaps remain for a broad mapping of APW, including improved PMF mapping, which would allow for adequate plastic waste management.

Efforts to map, detect, or extract plastic agricultural structures have been directed toward detecting PGH, and fewer articles have focused on PMF mapping (see Figure A5 in the Appendix). Lu et al. (2018) obtained 83.51% overall accuracy (OA), using data from the MODIS sensor to detect PMF. Hasituya et al. (2017found OA: 97.01%, producer accuracy (PA): 92.48%, and user accuracy (UA): 96.40%, with GaoFen-1 imagery. Xiong et al. (2019) detected PMF in large areas using a classification and regression tree on Sentinel-2 imagery, reaching an OA of 92.2%. Huang et al. (2022) used RGB images from unmanned aerial vehicle, achieving accuracies of around 90%. De Souza et al. (2024) also tested a temporal approach, reaching an OA of 99.7%. However, they analyzed a series of only three moments of the season. Although the streamlined time series presented by de Souza et al. (2024) was a great hypothesis to reduce computational processing and boost efficiency, it could also generate information loss, demanding knowledge and attention to balance efficient processing and relevant data retention. Here, we present a different proposal, testing DL models that consider the temporal relationship in a series with more images per season (11-12).

2. Methodology

The following subsections describe the process of mapping tomato PMF, including comparisons and analysis. The time series was used to capture intraseasonal changes and minimize misclassification between PMF and other land use and land cover (LULC), as indicated in Figure A1 in the Appendix. We trained and validated classifier algorithms using the sits package (Simoes et al., 2021) in R-4.3.1 (R Core Team, 2023).

2.1 Data

We used a processed image time series with a 16-day composite (S2-16D) obtained from Brazil Data Cube (BDC). The mentioned BDC time series came from Sentinel-2 images (Ferreira et al., 2020). The Copernicus Sentinel-2 mission is based on a constellation of two polar-orbiting satellites (2A and 2B) in the same sun-synchronous orbit at 786 km altitude (European Space Agency - ESA, 2023). The analysis used an S2-16D cube from July 2020 to July 2022, comprising four tomato seasons, each lasting around six months. In this period, we found 47 images in S2-16D, corresponding to three seasons with 12 and one with 11 images.

The process of PMF sampling entailed the visual identification and outlining of shapes on Sentinel-2 satellite images by an analyst. Sections encompassed regions of adjacent PMF polygons (refer to Figure A2 in the Appendix). These sections were further divided into smaller plots, each exhibiting a consistent color across its pixels. Subsequently, random points were generated solely within these plots to capture the spectral response in each band. In view of the challenges in obtaining a comprehensive sample set for other predominant classes within an area characterized by diverse LULC, we focused on binary classification - PMF or non-PMF. Non-PMF sampling was randomly performed outside the designated sections.

We incorporated the Plastic-Mulched Landcover Index (PMLI), proposed by Lu et al. (2014) and defined in Eq. 1, into S2-16D bands. Thus, the bands used in the classification were B02 (blue), B03 (green), B04 (red), B05 (red edge 1), B06 (red edge 2), B07 (red edge 3), B08 (NIR - near-infrared), B8A (NIR - near-infrared 2), B11 (SWIR 1 - shortwave infrared), B12 (SWIR 2), NDVI (Normalized Difference Vegetation Index), and PMLI.

$$PMLI = (B11 - B04)/(B11 + B04) \ , \qquad (1)$$

where B11 = SWIR 1 - shortwave infrared
B04 = red

2.2 Study Area

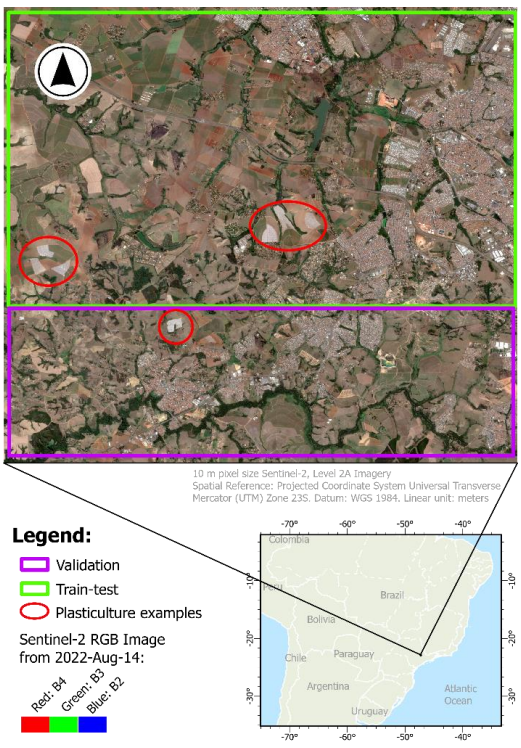

Figure 1. Study area and the segmentation of the ROI.

The region of interest (ROI) intersects six municipalities located in São Paulo, Brazil (Figure 1), and has approximately 300 km².

We divided the ROI into two segments, one for classifier training and testing and the other for validation. The ROI weather, according to the Köppen climate classification, is humid subtropical with a hot summer. Tomatoes grown with PMF in São Paulo have two harvests per year (hereafter named 1 for the first semester and 2 for the second).

The train-test section of the ROI led to a dataset with 59,094 samples (24,324 of PMF and 34,770 of non-PMF) for the four seasons. The validation section had 9,542 sample points and was used for model comparison of tuned and trained models. Since the sampling was imbalanced, we balanced the validation dataset using the function “sits_reduce_imbalance”, before the model comparison via evaluation metrics. The function randomly dropped points from the majority class and reduced the dataset to 4,476 points (1,500 of PMF and 2,976 of non-PMF).

2.3 Classification

We compared four pixel-based classifiers using the S2-16D data cube for PMF recognition. Table 1 shows the algorithms from the sits package tested for supervised classification: RF, MLP, L-TAE, and TCNN. Two algorithms do not explicitly consider the temporal structure of the time series (RF and MLP). In contrast, in L-TAE and TCNN algorithms, the temporal relations between observed values in a time series are considered. Refer to Figure A3 in the Appendix to see the learning curve of the best model.

Classifier	Abbr.	Class	References
Random Forest	RF	Trees Ensembles	Breiman (2001)
Multi-Layer Perceptron	MLP	Neural networks	Rosenblatt (1958) and Goodfellow et al. (2016)
Light Temporal Attention Encoder	L-TAE	Attention-based models	Garnot & Landrieu (2020)
Temporal Convolutional Neural Network	TCNN	Deep Neural networks	Pelletier et al. (2019)

Table 1. Classifiers compared for the PMF mapping task.

We employed hyperparameter tuning (HPT) for the DL models L-TAE and TCNN. Selected hyperparameters were tuned using a random search on values in the range specified in Table 2. We applied the algorithm “sits_tuning” from the sits package.

Classifier	Hyper parameter	Range	Best
L-TAE	lr	loguniform (10^{-2} - 10^{-4})	2.643573e-04
	weight_decay	loguniform (10^{-2} - 10^{-4})	5.718185e-07
TCNN	layers	(64, 64, 64) (128, 128, 128) (256, 256, 256)	(256,256,256)
	kernels	3/ 5/ 7	5
	dropout_rates	0.15/ 0.2/ 0.3/ 0.4	0.15
	lr	loguniform (10^{-2} - 10^{-4})	4.828950e-04
	weight_decay	loguniform (10^{-2} - 10^{-8})	1.268194e-04

Table 2. HPT for the DL classifiers.

2.4 Evaluation

To evaluate and compare the proposed ML classifiers, we adopted OA, kappa coefficient (κ), UA, PA, and F-score (F1). The metrics were calculated using a 6-fold cross-validation on the validation set.

For two classes, the OA can be defined as a binary classification test. That is, OA is equal to the proportion of right predictions among all instances validated (Eq. 2).

$$OA = \frac{TP+TN}{TP+FP+TN+FN}, \quad (2)$$

where TP = number of true positives
TN = number of true negatives
FP = number of false positives
FN = number of false negatives

The κ is a statistical measure used to quantify the level of agreement for mutually exclusive classes (Eq. 3).

$$\kappa = \frac{p_o - p_e}{1 - p_e} = \frac{2\times(TP\times TN - FP\times FN)}{(TP+FP)\times(FP+TN)+(TP+FN)\times(FN+TN)}, \quad (3)$$

where p_o = observed relative agreement
p_e = theoretical probability of random match

The UA is the complement of the Commission Error, corresponding to TP divided by all classified as positives (Eq. 4). The PA, also called Recall, is the complement of the Omission Error, the proportion of TP relative to the number of actual positives in the validation set (Eq. 5). F1 is the harmonic mean of UA and PA (Eq. 6), representing the class accuracy.

$$UA = Precision = \frac{TP}{TP+FP}, \quad (4)$$

$$PA = Recall = \frac{TP}{TP+FN}, \quad (5)$$

$$F1 = \frac{2}{UA^{-1}+PA^{-1}} = 2\times\frac{UA\times PA}{UA+PA} = \frac{2TP}{2TP+FP+FN}, \quad (6)$$

The last step was producing a classified map with the top classifier. The classified map was obtained from the output data cube, which consists of probability layers for each output class. These layers indicate the probability of each pixel belonging to a specific class. We visually evaluated the final map, identifying potential noise.

3. Results and Discussion

The dendrogram presented in Figure 2, using Ward linkage (Ward, 1963), also known as minimum variance linkage, indicates that the decision boundary is not very clear. It indicates possible confusion using a traditional classifier in a non-temporal approach, which we confirmed and show in Figure A1. We suggest that the solution to this problem involves increasing dimensionality (incorporating more information) or adopting a time series approach. In addition, we suggest adopting more robust classifiers capable of dealing with this difficulty, such as artificial neural networks.

This contribution has been peer-reviewed. The double-blind peer-review was conducted on the basis of the full paper.
https://doi.org/10.5194/isprs-annals-X-3-2024-101-2024 | © Author(s) 2024. CC BY 4.0 License.

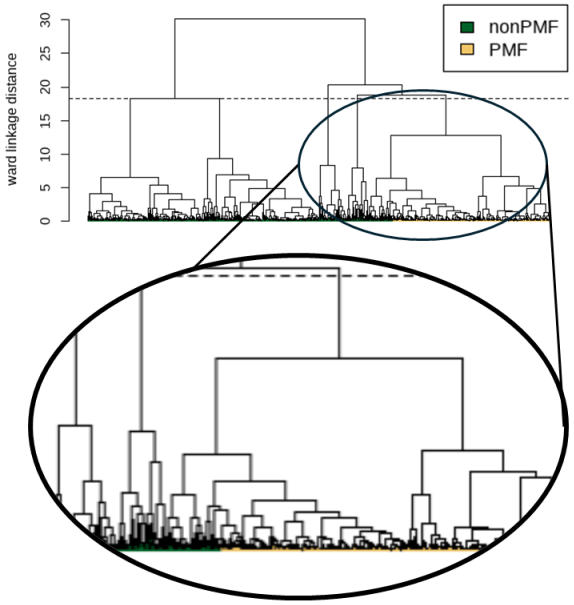

Figure 2. Dendrogram with Ward linkage distance for the PMF and non-PMF classes.

The mulching film presented spectral overlapping with some types of building roofs, as indicated in Figure 3, Figure A1, and also noted by Levin et al. (2007), D. Chen et al. (2023), and de Souza et al. (2024). The plastic is visible for a short period during the tomato PMF crop due to vegetation growth in the management carried out. Opportunely, as observed by de Souza et al. (2024), a distinct order of land cover delineates tomato cultivation with plastic films: bare soil > visible plastic film > growing vegetation > bare soil. This sequence within a time-series approach resolves the majority misclassification.

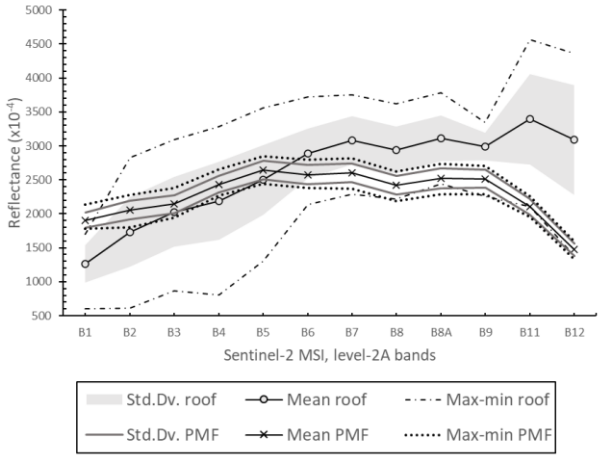

Source: de Souza et al. (2024)

Figure 3. Reflectance overlapping for PMF and urban roofs.

The best classifier was L-TAE (Table 3). It did not show FN or FP in the confusion matrix carried out in the validation dataset, which means 100% accuracy. In general, the time series approach presented outstanding metrics for PMF mapping. All the classifiers performed very well, and the obtained accuracies are comparable with the best works in the literature.

However, the variety of landscapes poses challenges for plastic film mapping. While the classifier may work well in specific regions, it can struggle with unknown backgrounds elsewhere or during different seasons (P. Zhang et al., 2022). Authors that utilized bands and indices to map agricultural plastics (Lu et al., 2018; Perilla & Mas, 2019) faced hurdles, including intricate landscapes, intra and interseasonal changes, and limited spatial resolution. The time series approach partially overcomes these difficulties.

	RF	MLP	TCNN	L-TAE
OA	0.9995	0.9993	0.9998	1.0
κ	0.9990	0.9985	0.9995	1.0
PA nonPMF	0.9993	0.9990	0.9997	1.0
PA PMF	1.0	1.0	1.0	1.0
UA nonPMF	0.9987	0.9980	0.9993	1.0
UA PMF	0.9997	0.9995	0.9998	1.0
F1 nonPMF	0.9990	0.9985	0.9995	1.0
F1 PMF	0.9998	0.9997	0.9999	1.0

Table 3. Classifiers’ metrics on the validation dataset.

The explicit consideration of the temporal structures contained in the architectures from DL classifiers had a less pronounced impact than expected. In other words, although the best classifier considered the temporal structure, RF and MLP did not and still showed similar accuracies. Referring to the metrics presented in Table 3, we must weigh the trade-offs. RF’s simplicity and efficiency make it an attractive choice, especially when computational resources are scarce. Conversely, TCNN and L-TAE’s potential benefits come at the expense of longer training times and higher computational costs.

We identified 248.5 ha (2.5 km²) of tomato PMF in the ROI for the 2022/1 season (Figure 4). The total area ranged from 180 (2021/1) to 343 ha (2022/2) throughout the assessed seasons (2020/2 - 2022/1), with the relocation of crops each season. The PMF area can potentially produce a substantial quantity of polyethylene (PE) APW.

Despite the excellent metrics, L-TAE presented some noise in the final classification map (Figure 4). Visually in the map, the classifier result looks worse than RF, for example. Given the presence of mixed pixels in images and the considerable data variability within each class, we could use the Bayesian smoothing parameter when generating the thematic map to overcome this noise common in pixel-based classification. This post-processing technique, decisive in refining the labels and improving the interpretability of the final output (Schindler, 2012; Xin Huang et al., 2014), is present in the “sits_label_classification” tool. We did not employ the smoothing, but it could be explored in future works as well as a better model assessment considering the noise in the final classification.

Another possibility for assessing the final map accuracy is to use the “sits_accuracy” function from the sits package. The function uses an area-weighted technique, following the procedure set by Olofsson et al. (2013). The area-weighted estimation is interesting because the two land-use classes are not evenly distributed in space.

The pixel-based approach and restricted sampling used have some bottlenecks, notwithstanding the excellent performance of the models. The use of PMF in tomatoes occurs in a specific time window. Therefore, it is crucial to perform future experiments incorporating other PMF crops to evaluate the outcomes in a multiclass task for comprehensive PMF mapping.

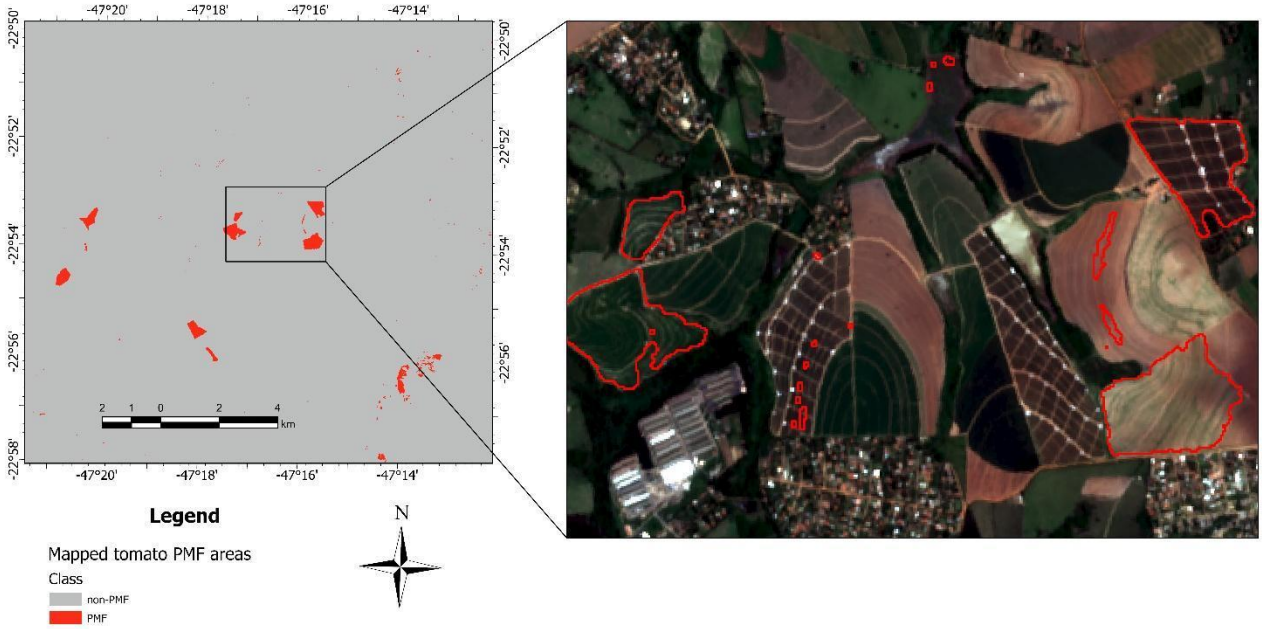

Figure 4. Example of tomato PMF areas mapped by the L-TAE in the ROI for the 2022/1 season.

We chose the tomato PMF as a case study because it has significant spatial mobility over seasons, posing an exciting challenge for RS detection. Growers strategically change cultivation locations to mitigate issues associated with pests and plant diseases. Then, the tomato plot will be in a different location for each season than the preceding season. The management also produces a substantial quantity of PE residue because the plastic films are semi-yearly renewed.

The RF classifier, in addition to delivering excellent metrics, allows an analysis of the importance of attributes (Figure 5) embedded in the function “plot(rfor_model)” (Camara et al., 2023; Simoes et al., 2021). Providing the minimum depth distribution for the top ten attributes from the RF analysis is an excellent way to illustrate the contribution and discriminative power of each attribute. In this context, attributes ranked in the top positions, with lower mean minimum depth values, suggest that they were more frequently and earlier selected to partition the trees within the forest. The B02 (wavelength 492.1–496.6 nm) and the PMLI index, both based on the second date of the time series, were critical for distinguishing PMF. B02 has high reflectance and minimal spectral overlap with other land uses. PMLI because it is an index devoted to the identification of plastic mulching that combines SWIR1 (B11) and red (B04) bands.

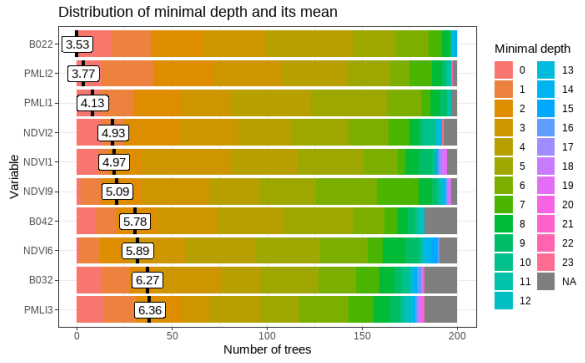

Figure 5. Attribute importance for PMF classification obtained from the RF model.

The spectral identity of PMFs (refer to Figure A4 in the Appendix) is influenced by the polymer and additives used in industrial processing, transparency, color, and thickness (Veettil et al., 2023). The pattern shown by bands and indices over time forms their distinctiveness. Some of the bands in the graph (Figure A4) presented multicollinearity between them, indicating that they ended up not providing extra information. Figures 5 and A4 suggest that a time series model using only one band of the visible spectrum (RGB), one from SWIR, PMLI, and NDVI could be able to map the PMF, as other bands were not observed among the most important ones and considering the collinearity among RBG bands. This configuration can be explored in future studies.

4. Conclusions

PMF mapping is very pertinent to support circularity. The development of plastic for agricultural applications is criticized for posing some environmental concerns despite its benefits for food production. Combining methodologies developed by different authors, we provided a successful model for PMF classification using the sits. The time series with selected bands and indices proposed in our research accurately mapped the PMF class at a regional scale. The pixel-based approach was not affected by spatial distribution. Furthermore, we compared four ML classifiers, where L-TAE was the most accurate. L-TAE's ability to work with the temporal domain explains its better performance for classifying PMF.

Considering the challenges mentioned in the introduction, we have contributed to overcoming some of them. Variations in pigment, spectral properties, and urban confusion were resolved by using spectral bands and PMLI in a time series, which was essential to defining the PMF's characteristic identity. Due to the Sentinel-2A data restriction, the challenges of accurate segmentation and area estimation caused by limited spatial resolution have not been completely resolved.

Accurate data about APW location and estimated quantities are indispensable for subsiding regional development and public

policies. In the established ROI, we identified around 250 ha of tomato PMF per season, capable of generating a significant volume of APW.

Acknowledgments

This study was financed by the Brazilian National Council for Scientific and Technological Development (CNPq) with process no. 125120/2023-0 and 305412/2023-0, Dow Ilimite-se/Unicamp (Process no. 01-P-416/2024), Braskem S.A., and the São Paulo Research Foundation (FAPESP) in process no. 2021/05251-8 and 2024/06854-6.

We thank the INPE BDC & SITS teams for the R package and data cube access and the Andrade Brothers' farm for access to the PMF areas. We want to extend our appreciation to the reviewers for their valuable contributions.

References

Afxentiou, N., Georgali, P. Z. M., Kylili, A., & Fokaides, P. A., 2021. Greenhouse agricultural plastic waste mapping database. *Data in Brief*, 34, 106622. doi.org/10.1016/J.DIB.2020.106622

Agüera, F., Aguilar, F. J., & Aguilar, M. A., 2008. Using texture analysis to improve per-pixel classification of very high resolution images for mapping plastic greenhouses. *ISPRS Journal of Photogrammetry and Remote Sensing*, 63(6):635–646. doi.org/10.1016/j.isprsjprs.2008.03.003

Blanco, I., Loisi, R. V., Sica, C., Schettini, E., & Vox, G., 2018. Agricultural plastic waste mapping using GIS. A case study in Italy. *Resour. Conserv. Recycl.*, 137, 229–242. doi.org/10.1016/j.resconrec.2018.06.008

Breiman, L.,2001. Random forests. *Machine Learning*, 45(1):5–32. doi.org/10.1023/A:1010933404324

Camara, G., Simoes, R., Souza, F., Peletier, C., Sanchez, A., Andrade, P. R., Ferreira, K., & Queiroz, G., 2023. *sits: Satellite Image Time Series Analysis on Earth Observation Data Cubes*. Retrieved July 2, 2024, from e-sensing.github.io/sitsbook

Chen, D., Ma, A., Zheng, Z., & Zhong, Y., 2023. Large-scale agricultural greenhouse extraction for remote sensing imagery based on layout attention network: A case study of China. *ISPRS Journal of Photogrammetry and Remote Sensing*, 200:73–88. doi.org/10.1016/J.ISPRSJPRS.2023.04.020

de Souza, M. F., Lamparelli, R. A. C., Oliveira, M. H. S., Nogueira, G. P., Bliska, A., & Franco, T. T., 2024. Remote sensing detection of plastic-mulched farmland using a temporal approach in machine learning: case study in tomato crops. *ESPR*. https://doi.org/10.1007/s11356-024-35026-7

Dimitrovski, I., Kitanovski, I., Kocev, D., & Simidjievski, N., 2023. Current trends in deep learning for Earth Observation: An open-source benchmark arena for image classification. *ISPRS Journal of Photogrammetry and Remote Sensing*, 197:18–35. doi.org/10.1016/J.ISPRSJPRS.2023.01.014

European Space Agency - ESA, 2023. *S2 Mission.* Copernicus. sentinels.copernicus.eu/web/sentinel/missions/sentinel-2

Ferreira, K. R. et al., 2020. Earth Observation Data Cubes for Brazil: Requirements, Methodology and Products. *Remote Sensing*, 12(24), 4033; doi.org/10.3390/rs12244033

Food and Agriculture Organization - FAO, 2021. *Assessment of agricultural plastics and their sustainability: A call for action*. FAO. doi.org/10.4060/cb7856en

Garnot, V.S.F., Landrieu, L., 2020. Lightweight Temporal Self-attention for Classifying Satellite Images Time Series. In: Lemaire, V., Malinowski, S., Bagnall, A., Guyet, T., Tavenard, R., Ifrim, G. (eds). Int. Wksp. Adv. Anal. Learning Temp. Data, AALTD 2020. *Lect. Notes Comp. Science*, vol 12588. Springer, Cham. doi.org/10.1007/978-3-030-65742-0_12

Gao, N., Wei, Y., Zhang, W. W., Yang, B., Shen, Y., Yue, S., & Li, S., 2022. Carbon footprint, yield and economic performance assessment of different mulching strategies in a semi-arid spring maize system. *Sci. Total Environ*, 826. https://doi.org/10.1016/j.scitotenv.2022.154021

Ghaffar, I., Rashid, M., Akmal, M., & Hussain, A., 2022. Plastics in the environment as potential threat to life: an overview. *Environmental Science and Pollution Research*, 29(38):56928–56947. doi.org/10.1007/s11356-022-21542-x

Goodfellow I., Y. Bengio, and A. Courville, 2016. *Deep Learning*. MIT Press. www.deeplearningbook.org/

Hasituya, Chen, Z., Wang, L., & Liu, J., 2017. Selecting appropriate spatial scale for mapping plastic-mulched farmland with satellite remote sensing imagery. *Remote Sensing*, 9(3). doi.org/10.3390/rs9030265

Hofmann, T., Ghoshal, S., Tufenkji, N., Adamowski, J. F., Bayen, S., Chen, Q., Demokritou, P., Flury, M., Hüffer, T., Ivleva, N. P., Ji, R., Leask, R. L., Maric, M., Mitrano, D. M., Sander, M., Pahl, S., Rillig, M. C., Walker, T. R., White, J. C., & Wilkinson, K. J., 2023. Plastics can be used more sustainably in agriculture. *Communications Earth and Environment*, 4(1):332. doi.org/10.1038/s43247-023-00982-4

Hong, R., Xiao, B., Yan, H., Liu, J., Liu, P., & Song, Z., 2023. Multitemporal greenhouse mapping for high-resolution remote sensing imagery based on an improved YOLOX. *Computers and Electronics in Agriculture*, 206, 107689. doi.org/10.1016/j.compag.2023.107689

Huang, D., Zhou, Z., Zhang, Z., Zhu, M., Peng, R., Zhang, Y., Li, Q., Xiao, D., & Hu, L., 2022. Extraction of agricultural plastic film mulching in karst fragmented arable lands based on unmanned aerial vehicle visible light remote sensing. *J. Appl. Remote Sens.*, 16(03). doi.org/10.1117/1.JRS.16.036511

Huo, Y., Dijkstra, F. A., Possell, M., & Singh, B., 2022. Ecotoxicological effects of plastics on plants, soil fauna and microorganisms: A meta-analysis. *Environmental Pollution*, 310:119892. doi.org/10.1016/j.envpol.2022.119892

Institute for Processing Empty Packages – inpEV, 2023. *Sustainability Report 2022*. inpev.org.br/relatorio-sustentabilidade/2022/en

Kruse, C., Boyda, E., Chen, S., Karra, K., Bou-Nahra, T., Hammer, D., Mathis, J., Maddalene, T., Jambeck, J., & Laurier, F., 2023. Satellite monitoring of terrestrial plastic waste. *PLoS One*, 18(1), e0278997. doi.org/10.1371/journal.pone.0278997

Levin, N., Lugassi, R., Ramon, U., Braun, O., & Ben-Dor, E., 2007. Remote sensing as a tool for monitoring plasticulture in

agricultural landscapes. *Int. J. Remote Sens.*, 28(1):183–202. doi.org/10.1080/01431160600658156

Lin, Y., Zhang, J., Jiang, Z., & Tang, Y., 2023. YOLOv5-Atn: An Algorithm for Residual Film Detection in Farmland Combined with an Attention Mechanism. *Sensors*, 23(16), 7035. doi.org/10.3390/S23167035

Liu, X., & Xin, L., 2023. Spatial and temporal evolution and greenhouse gas emissions of China’s agricultural plastic greenhouses. *Sci. Total Environ.*, 863:160810. doi.org/10.1016/J.SCITOTENV.2022.160810

Lu, L., Di, L., & Ye, Y., 2014. A decision-tree classifier for extracting transparent plastic-mulched Landcover from landsat-5 TM images. *IEEE J. Sel. Top. Appl. Earth Obs. Remote Sens.*, 7(11):4548–4558. doi.org/10.1109/JSTARS.2014.2327226

Lu, L., Huang, Y., Di, L., & Hang, D., 2018. Large-scale subpixel mapping of landcover from MODIS imagery using the improved spatial attraction model. *J. Appl. Remote Sens.*, 12(04):1. doi.org/10.1117/1.jrs.12.046017

Ni, Y., Richter, G. M., Mwabonje, O. N., Qi, A., Patel, M. K., & Woods, J., 2021. Novel integrated agricultural land management approach provides sustainable biomass feedstocks for bioplastics and supports the UK’s “net-zero” target. *Environ. Res. Lett.*, 16(1). doi.org/10.1088/1748-9326/abcf79

Olofsson, P., Foody, G. M., Stehman, S. V. & Woodcock, C. E., 2013. Making better use of accuracy data in land change studies: Estimating accuracy and area and quantifying uncertainty using stratified estimation. *Remote Sens. Environ.*, 129, 122–131. doi.org/10.1016/j.rse.2012.10.031

Pelletier, C., Webb, G., & Petitjean, F., 2019. Temporal Convolutional Neural Network for the Classification of Satellite Image Time Series. *Remote Sensing*, 11(5), 523. doi.org/10.3390/rs11050523

Perilla, G. A., & Mas, J. F., 2019. High-resolution mapping of protected agriculture in Mexico, through remote sensing data cloud geoprocessing. *Eur. J. Remote Sens.*, 52(1):532–541. doi.org/10.1080/22797254.2019.1686430

R Core Team, 2023. *A Language and Environment for Statistical Computing*. R Foundation for Statistical Computing, Vienna, Austria. www.R-project.org

Rosenblatt, F., 1958. The perceptron: A probabilistic model for information storage and organization in the brain. *Psychological Review*, 65(6):386–408. doi.org/10.1037/h0042519

Simoes, R., Camara, G., Queiroz, G., Souza, F., Andrade, P. R., Santos, L., Carvalho, A., & Ferreira, K., 2021. Satellite Image Time Series Analysis for Big Earth Observation Data. *Remote Sensing*, 13(13), 2428. doi.org/10.3390/rs13132428

Schindler, K., 2012. An Overview and Comparison of Smooth Labeling Methods for Land-Cover Classification. *IEEE Transactions on Geoscience and Remote Sensing*, 50(11), 4534–4545. doi.org/10.1109/TGRS.2012.2192741

United Nations - UN, 2021. *Population, food security, nutrition and sustainable development*. UN Economic and Social Council. undocs.org/en/E/CN.9/2021/2

Veettil, B. K., Van, D. D., Quang, N. X., Hoai, P. N., 2023. Remote sensing of plastic-covered greenhouses and plastic-mulched farmlands: Current trends and future perspectives. *Land Degrad. Dev.*, 34(3):591–609. doi.org/10.1002/LDR.4497

Ward, J. H., 1963. Hierarchical Grouping to Optimize an Objective Function. *J. Am. Stat. Assoc.*, 58 (301): 236–244. doi.org/10.1080/01621459.1963.10500845

Xin Huang, Qikai Lu, Liangpei Zhang, & Plaza, A., 2014. New Postprocessing Methods for Remote Sensing Image Classification: A Systematic Study. *IEEE Trans. Geosci. Remote Sens.*, 52(11), 7140–7159. doi.org/10.1109/TGRS.2014.2308192

Xiong, Y., Zhang, Q., Chen, X., Bao, A., Zhang, J., & Wang, Y., 2019. Large Scale Agricultural Plastic Mulch Detecting and Monitoring with Multi-Source Remote Sensing Data: A Case Study in Xinjiang, China. *Remote Sensing*, 11(18):2088. doi.org/10.3390/rs11182088

Zhang, P., Du, P., Guo, S., Zhang, W., Tang, P., Chen, J., & Zheng, H., 2022. A novel index for robust and large-scale mapping of plastic greenhouse from Sentinel-2 images. *Remote Sensing of Environment*, 276: 113042. doi.org/10.1016/J.RSE.2022.113042

Zhao, G. X., Li, J., Li, T., Yue, Y. D., & Warner, T., 2004. Utilizing landsat TM imagery to map greenhouses in Qingzhou, Shandong Province, China. *Pedosphere*, 14(3):363–369. pedosphere.issas.ac.cn/trqen/ch/reader/view_abstract.aspx?file_no=20040312

Appendix

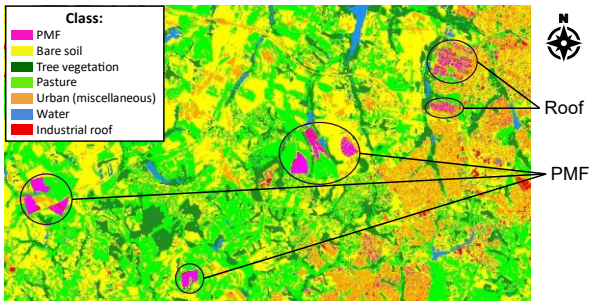

Source: de Souza et al. (2024)

Figure A1. Result of a non-temporal multiclass model using RF classifier. The circles highlight the confusion between PMFs and roofs.

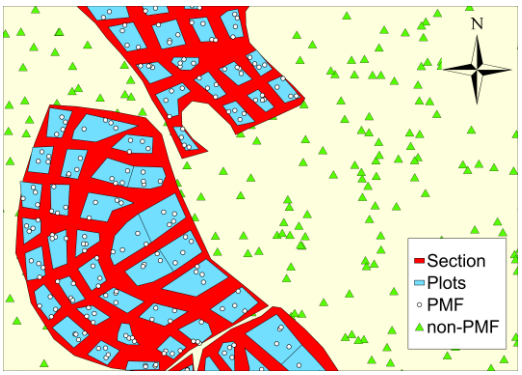

Figure A2. Sampling plan.

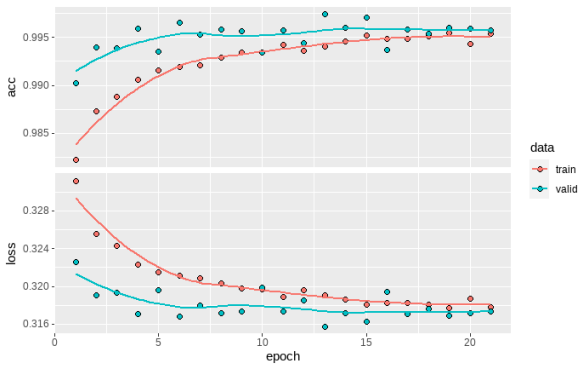

Figure A3. Learning curve for the L-TAE classifier.

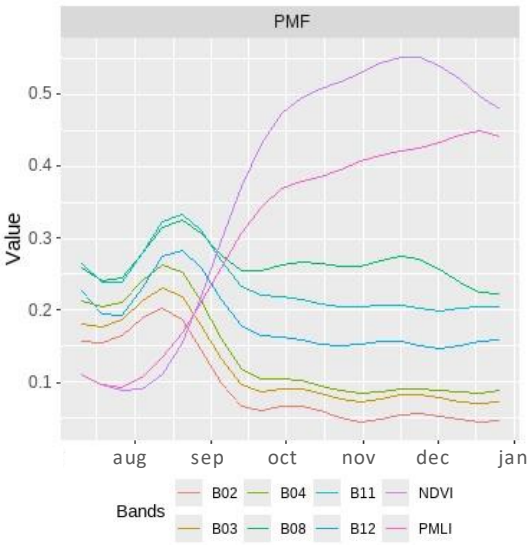

Figure A4. Spectral response of selected bands, PMLI, and NDVI over time for the PMF class.

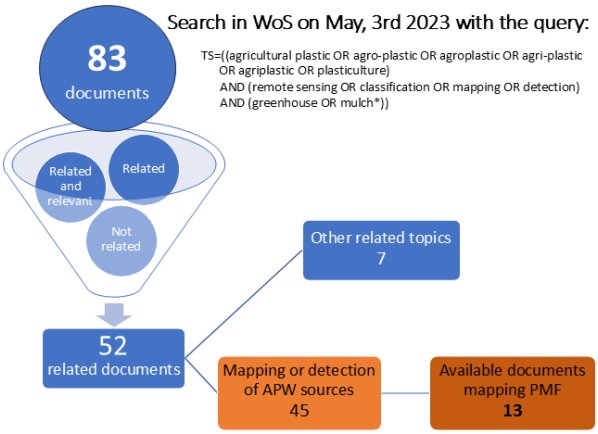

Figure A5. Results of a systematic review in Web of Science.